PHYSICAL REVIEW B VOLUME 47, NUMBER 8 15 FEBRUARY 1993-II

Effects of the Coulomb interaction on the optical spectra of quantum wires

S. Glutsch and F. Bechstedt
Friedrich-Schiller-Universität, Institut für Festkörpertheorie und Theoretische Optik, Max-Wien-Platz 1, O-6900 Jena, Germany
(Received 28 May 1992; revised manuscript received 28 September 1992)

We investigate theoretically excitonic effects on the optical properties of quantum-wire structures. The spatial nonlocal optical susceptibility is expressed in terms of electron-hole pair wave functions and energies. The corresponding two-particle equation is numericllay solved assuming a complete vertical confinement. The resulting exciton energies and the oscillator strengths are studied versus the wire confinement. The interplay of Coulomb attraction, center-of-mass quantization, and confinement of the internal motion is discussed. Very recent luminescence spectra for quantum-wire arrays fabricated by means of laser-induced cation interdiffusion, which show a variety of narrow exciton lines, can be interpreted.

I. INTRODUCTION

The spectroscopy of optical interband transitions across the band gap is a powerful method used to study the electronic structure, the mutual interaction of excited electrons (e) and holes (h), and the coupling of these carriers with other elementary excitations in semiconductors and semiconductor microstructures. Very interesting systems in this respect are quantum wires and quantum-wire (QW) arrays. In such quasi-one-dimensional (1D) structures, made by epitaxial growth of III-V semiconductor layers and nanostructuring techniques, quantum confinement in two dimensions is realized. One has the interesting case of a quasi-1D carrier motion and strong optical anisotropy.

Some effects attributed to quantum confinement and anisotropy have already been observed in photoluminescence and photoluminescence excitation spectra[1-8] and their dependence on light polarization.[3-6] Partially, such measurements are also time resolved.[7,9] Most of the QW structures studied by optical methods have been prepared by starting from GaAs-$Al_xGa_{1-x}As$ layered systems and employing modern lithographic techniques.[10] Commonly, they are combined with etching techniques which produce rough surfaces of the wire structures resulting in peaks that are broader than those of the corresponding 2D system.[6] Very recently, more perfect QW structures have been manufactured via Al/Ga interdiffusion due to local heating by means of a focused laser beam.[8] The quality of these samples is characterized by excitonic luminescence lines that are smaller as in the 2D case.

There are several theoretical papers about QW systems. The calculations started with the single-particle energy levels in the conduction and valence bands of the 1D structures.[11-15] The corresponding 1D interband transitions have been commonly studied only in the parabolic approximation for the valence bands.[16-18] Now it is shown[19-22] that a proper treatment of the valence bands leads not only to a modification of transition energies and oscillator strengths, but is especially necessary to describe the light polarization anisotropy with respect to the wire structure.

In the optical absorption and luminescence spectra, excitonic effects play an important role, particularly in the low-dimensional QW systems. However, in contrast to the exact 3D or 2D case,[23,24] to our knowledge, no unified picture of the Coulomb effects in this spectra has been presented. Only binding energies of the excitons have been calculated[25-29] and Sommerfeld factors of exact 1D systems with modified Coulomb potentials have been studied.[30]

In the present paper we develop the theory for optical absorption and luminescence spectra of quantum wires including the Coulomb attraction of an electron and hole excited by a photon. This paper is organized as follows. The basic theory is given in Sec. II. We define the relevant optical quantities starting from a nonlocal susceptibility. It is related to the wave functions and energies of the electron-hole pair equation. In Sec. III, an explicit solution of the electron-hole problem in a single wire is given within the harmonic confinement model and for strong confinement in the growth direction of the structure. The quantization of the center-of-mass motion and the influence of the confinement on the nominal 2D excitons are studied separately. We discuss exciton energies, wave functions, and oscillator strengths versus the wire width. Reflecting the experimental situation of Ref. 8, luminescence spectra are calculated in Sec. IV. Applying realistic wire confinement potentials with varying width as well as height and varying wire distance we try to reproduce experimental spectra. Finally, in Sec. V a summary is given.

II. THEORETICAL BASIS

A. Relation of optical spectra and two-particle properties

For systems where the spatial dispersion in the photon propagator is especially negligible, and in the long-wavelength limit, optical properties can be expressed in terms of the frequency-dependent optical susceptibility

$$\chi(\omega)=\int_V d^3\mathbf{x}\int_V d^3\mathbf{x}'\chi(\mathbf{x},\mathbf{x}';\omega)\ , \tag{1}$$

where the spatial integration runs over the optically active volume V. For example, the absorption coefficient $\alpha(\omega)$ of the transmitted light and the intensity $I(\omega)$ of the luminescence light emitted spontaneously, defined as photon energy per energy interval, volume, and time, can be related to its imaginary part by[31]

$$\begin{aligned}\alpha(\omega)&=\frac{\omega}{cn(\omega)}\mathrm{Im}\chi(\omega)\ ,\\ I(\omega)&=\frac{\omega^4 n(\omega)}{\pi^2 c^3}g(\hbar\omega-\Delta\mu)\mathrm{Im}\chi(\omega)\ ,\end{aligned} \tag{2}$$

with the index of refraction $n(\omega)$ and the Bose function $g(\hbar\omega)$. $\Delta\mu$ denotes the sum of the quasichemical potentials for electrons and holes with respect to the corresponding band edges.[32] In the case of photoluminescence, these chemical potentials are driven by exiting laser light.

In general, the description of the optical properties of a QW array requires more complicated formulas as in Eq. (2). The electrodynamical problem for the underlying layered structure, that is additionally laterally structured, has to be solved. Moreover, the QW array is commonly finite. A second problem in the description of the optical spectra concerns their polarization dependence. Without Coulomb interaction the effects of polarization and grating structure of the sample are reasonably studied.[19–22] We start from allowed optical transition and omit these dependences in our explicit calculations.

The space-dependent optical susceptibility appearing in Eq. (1) can be directly related to electron-hole-pair wave functions $\Phi_\alpha(\mathbf{x}_e,\mathbf{x}_h)$ and energies E_α with α as the complete set of quantum numbers for the two-particle problem by[31,33]

$$\chi(\mathbf{x},\mathbf{x}';\omega)=\frac{2}{\varepsilon_0}|\boldsymbol{\mu}|^2\sum_\alpha\frac{\Phi_\alpha(\mathbf{x},\mathbf{x})\Phi_\alpha^*(\mathbf{x}',\mathbf{x}')}{E_\alpha-\hbar(\omega+i\Gamma)}\ . \tag{3}$$

In practice, the dipole-matrix elements $|\boldsymbol{\mu}|$ contain the complete polarization-vector dependence of the problem. The optical dipole transition is assumed to be allowed and nearly state independent. ε_0 denotes the vacuum dielectric constant and Γ indicates the damping of the electron-hole pairs. The two-particle wave functions are orthonormalized and complete. In the framework of the effective-mass approximation and masses m_e (m_h) of electrons (holes), they obey a Schrödinger equation of the form

$$\left\{\sum_{i=e,h}\hat{H}_i(\mathbf{x}_i)-\frac{e^2}{4\pi\varepsilon_0\varepsilon|\mathbf{x}_e-\mathbf{x}_h|}\right\}\Phi_\alpha(\mathbf{x}_e,\mathbf{x}_h)=E_\alpha\Phi_\alpha(\mathbf{x}_e,\mathbf{x}_h)\ , \tag{4}$$

where electrons and holes interact by a Coulomb potential screened by a relative static dielectric constant ε of the underlying semiconductor material forming the wires. The complications in the screening due to the realistic spatial structure of the system[34] are avoided assuming that the dielectric constants of wire and barrier materials are not so very different as in the case of GaAs and $Al_xGa_{1-x}As$. The single-particle Hamiltonians for electron or hole are ($i=e,h$)

$$\hat{H}_i(\mathbf{x}_i)=-\frac{\hbar^2}{2}\nabla_{\mathbf{x}_i}\frac{1}{m_i}\nabla_{\mathbf{x}_i}+V_{iy}(y_i)+V_{iz}(z_i)\ . \tag{5}$$

For the sake of simplicity, the potential that confines carriers in the quasi-1D structures is written as a sum. The confinement in growth direction z of the layered structure is represented by the potentials $V_{iz}(z_i)$. The wires are assumed to be directed parallel to the x axis. The quantization within the wires is given by the potentials $V_{iy}(y_i)$.

B. Specification of hole states and confinement

The valence-band structure of bulk zinc-blende materials forming the microstructures under consideration is rather complicated. Despite spin-orbit interaction, the top of the Γ_8 valence band is fourfold degenerated.[35] In microstructures this degeneracy is partially lifted and heavy- and light-hole states are generally mixed. Nevertheless, starting from the well-defined energetical separation we study a heavy-hole valence-band to conduction-band transition. The relevant heavy-hole mass follows from the Luttinger parameters[35,36] in axial approximation[37] as $m_{h\|}=0.491m$ in accordance with strong confinement in z direction due to the well. The mass of the electron in the Γ_6 conduction-band minimum is $m_e=0.068m$.[38]

For completely vanishing confinement with $V_{iy}(y_i)=V_{iz}(z_i)=0$, i.e., in the exact 3D case, Eq. (4) is fully separable into equations for the free center-of-mass motion and for the internal motion of the excitons. From expressions (1) and (3) the famous Elliott formula[23] follows for the optical susceptibility $\chi(\omega)$ including fully the excitonic effects. The corresponding problem for the microstructures, i.e., the quasi-2D or the quasi-1D cases, can be only solved approximately. The other exactly solvable case is that of strong confinement in the xy plane, i.e., the exact 2D case.[24] The ideal limit of the 1D electron-hole system, namely infinitesimal wire cross sections and perfect confinement, leads to several pathological features of the excitons below the band edge[39,40] as, e.g., the divergence of the binding energy of the lowest-energy exciton.

Realistic QW systems can only be treated in an approximate manner. We start with the assumption of strong confinement $V_{iz}(z_i)(i=e,h)$ of electrons and holes in the growth direction z. More strictly speaking, the thickness of the GaAs quantum well in the layered structure, that is laterally structured to prepare the QW's, is assumed to be so small that the optical intersubband transitions in the quasi-2D system are energetically well separated. In the considered energy region we can restrict ourselves only to the lowest electron and hole subbands. If the confinement in these states is strong enough it is sufficient to consider only the 2D carrier motion in the xy plane, i.e., one has

$$\Phi_\alpha(\mathbf{x}_e,\mathbf{x}_h)=\varphi_\alpha(\mathbf{r}_e,\mathbf{r}_h)\delta^{1/2}(z_e)\delta^{1/2}(z_h) \tag{6}$$

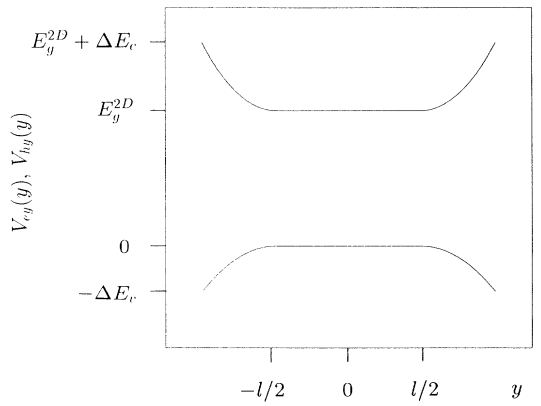

FIG. 1. Electron and hole confinement potentials $V_{iy}(y)$ $(i=e,h)$ for a single quantum wire parallel x in the xy plane. The well depths are identified with the corresponding band discontinuities ΔE_c and ΔE_v. The energetic distance of the well bottoms is the energy E_g^{2D} of the underlying subband transition. The bottom width l and the total width of the well are assumed to be identical for electrons and holes. The particular form of the potentials allows the consideration of the limiting cases of harmonic confinement ($l=0$) and square-well potential ($l=$total width).

with the radius vector $\mathbf{r}$ in this plane. Equations (4) and (5) change over into

$$\left\{E_g^{2D}+\sum_{i=e,h}H_i(\mathbf{r}_i)-\frac{e^2}{4\pi\varepsilon_0\varepsilon|\mathbf{r}_e-\mathbf{r}_h|}\right\}\varphi_\alpha(\mathbf{r}_e,\mathbf{r}_h)=E_\alpha\varphi_\alpha(\mathbf{r}_e,\mathbf{r}_h)\ , \tag{7}$$

$$H_i(\mathbf{r}_i)=-\frac{\hbar^2}{2m_{i\parallel}}\Delta_i+V_{iy}(y_i)\ ,$$

where E_g^{2D} describes the optical transition energy in the underlying quantum-well structure including the effect of the strong quantization due to $V_{iz}(z_i)$ on the energies. The asymptotic form of the 2D Coulomb potential in Eq. (7) follows within the model of complete well confinement. It gives rise to small overestimation of the binding energies of the lower exciton states.

Typical potentials $V_{iy}(y_i)$ used later in the numerical calculations are shown for a single wire in Fig. 1. Potential forms of Fig. 1 allow the transition between the square-wire and parabolic-wire potentials.

C. Approximate decoupling of center-of-mass and internal exciton motion

Without wire confinement, i.e., $V_{iy}(y_i)\equiv 0$, Eq. (7) exactly describes the 2D exciton,[24] more strictly the motion of a Coulomb-correlated electron-hole pair in the xy plane. That means that in the limit of subband quantization, small compared to the 2D exciton binding energy, the natural coordinates of the problem are the relative (rel) coordinates and the center-of-mass (c.m.) coordinates,

$$\mathbf{r}=\mathbf{r}_e-\mathbf{r}_h\ ,$$
$$\mathbf{R}=\frac{m_{e\parallel}\mathbf{r}_e+m_{h\parallel}\mathbf{r}_h}{m_{e\parallel}+m_{h\parallel}}\ , \tag{8}$$

with $\mathbf{r}=(x,y)$ and $\mathbf{R}=(X,Y)$. Considering the Coulomb effects in the optical spectra, we apply these coordinates, since the typical wire width realized experimentally is larger than the Bohr radius of the exciton. Introducing the electron-hole reduced mass $\mu=m_{e\parallel}m_{h\parallel}/M$ and the total mass $M=m_{e\parallel}+m_{h\parallel}$, the two-particle Hamiltonian in Eq. (7) can be written as

$$\begin{aligned}\sum_{i=e,h}H_i(\mathbf{r}_i)-\frac{e^2}{4\pi\varepsilon_0\varepsilon|\mathbf{r}_e-\mathbf{r}_h|}&=-\frac{\hbar^2}{2M}\frac{d^2}{dX^2}+H_{\text{c.m.}}(Y)\\&\quad+H_{\text{int}}(Y,y)\\&\quad+H_{\text{rel}}(\mathbf{r})\ ,\end{aligned}$$

$$H_{\text{c.m.}}(Y)=-\frac{\hbar^2}{2M}\frac{d^2}{dY^2}+V_{\text{c.m.}}(Y)\ ,$$

$$\begin{aligned}H_{\text{int}}(Y,y)&=V_{ey}\left[Y+\frac{m_{h\parallel}}{M}y\right]\\&\quad+V_{hy}\left[Y-\frac{m_{e\parallel}}{M}y\right]\\&\quad-V_{\text{c.m.}}(Y)-V_{\text{rel}}(y)\ ,\end{aligned} \tag{9}$$

$$H_{\text{rel}}(\mathbf{r})=-\frac{\hbar^2}{2\mu}\Delta_{\mathbf{r}}+V_{\text{rel}}(y)-\frac{e^2}{4\pi\varepsilon_0\varepsilon|\mathbf{r}|}\ .$$

The new confinement potentials for the center-of-mass and relative motions

$$\begin{aligned}V_{\text{c.m.}}(Y)&=V_{ey}(Y)+V_{hy}(Y)\ ,\\V_{\text{rel}}(y)&=V_{ey}\left[\frac{M_{h\parallel}}{M}y\right]+V_{hy}\left[-\frac{m_{e\parallel}}{M}y\right]\ ,\end{aligned} \tag{10}$$

are chosen so that they give the most convenient splitting in the case of purely harmonic confinement $V_{iy}(y_i)=\frac{1}{2}m_{i\parallel}\omega_i^2y_i^2$ $(i=e,h)$.[41–43] It has been shown that such harmonic confinement seems to be a reasonable approach to the description of the wire quantization. This model has been already successfully applied to the dielectric properties[43–45] and coherent optical phenomena[46] of QW systems.

Unfortunately, the eigenvalue problem defined by the Hamiltonian in Eq. (9) is, in general, not separable in center-of-mass and relative coordinates. Apart from the limiting cases $Y=0$ or $y=0$, exact separation happens only for harmonic confinement and equal quantization energies $\omega_e=\omega_h$ for electron and hole.[47] Only the free motion of the center of mass in the x direction can be exactly treated. This motion can be separated from the two-particle wave function and characterized by a 1D wave vector K as the good quantum number ($\alpha=\hat{\alpha}K$),

$$\varphi_\alpha(\mathbf{r}_e,\mathbf{r}_h)=\frac{1}{\sqrt{L_x}}e^{iKX}\hat{\varphi}_{\hat{\alpha}}(Y,\mathbf{r})\ , \tag{11}$$

where the characteristic length L_x of the wires is intro-

duced. The center-of-mass motion perpendicular to the wires is essentially given by a Schrödinger equation,

$$H_{\text{c.m.}}(Y)\Phi_N(Y)=\varepsilon_N\Phi(Y) , \tag{12}$$

with energy eigenvalues ε_N and N as the quantum number of this motion. We expand the wave functions $\hat{\varphi}_{\hat{\alpha}}(Y,\mathbf{r})$ in terms of the complete and orthonormalized eigenfunctions of the Hamiltonian $H_{\text{c.m.}}(Y)$ by

$$\hat{\varphi}_{\hat{\alpha}}(Y,\mathbf{r})=\sum_N C^N_{\hat{\alpha}}(\mathbf{r})\Phi_N(Y) . \tag{13}$$

For the expansion coefficients depending on the relative coordinates of the electron and hole, one derives a coupled set of differential equations from Eq. (7). With Eqs. (9)–(13) it follows that

$$\sum_{N'}\left\{\left[H_{\text{rel}}(\mathbf{r})+E_g^{\text{2D}}+\frac{\hbar^2K^2}{2M}+\varepsilon_N-E_{\hat{\alpha}}(K)\right]\delta_{NN'}+W_{NN'}(y)\right\}C^{N'}_{\hat{\alpha}}(\mathbf{r})=0 ,$$
$$W_{NN'}(y)=\int_{-\infty}^{+\infty}dY\Phi^*_N(Y)H_{\text{int}}(Y,y)\Phi_{N'}(Y) . \tag{14}$$

In our numerical calculations we have found that for the wire widths being relevant in the optical experiments, the off-diagonal elements $W_{NN'}(y)(N\neq N')$ of the additional confinement potential for the internal exciton motion perpendicular to the wires are negligible. Then N is nearly a good quantum number with the restriction that the internal motion of the excitons depends again on the parameter N,

$$\{H_{\text{rel}}(\mathbf{r})+W_{NN}(y)\}C^N_{\hat{\alpha}}(\mathbf{r})=\varepsilon^N_{\hat{\alpha}}C^N_{\hat{\alpha}}(\mathbf{r}) ,$$
$$\varepsilon^N_{\hat{\alpha}}=E_{\hat{\alpha}}(K)-E_g^{\text{2D}}-\frac{\hbar^2K^2}{2M}-\varepsilon_N , \tag{15}$$

where the abbreviation $\varepsilon^N_{\hat{\alpha}}$ is introduced. The neglect of off-diagonal elements $N\neq N'$ seems to be crucial. In fact, their influence increases for decreasing wire widths. On the other hand, for wire widths larger or equal to the exciton radius the coupling effects remain small and the principal behavior of the related spectra is not changed. The validity of that assumption is confirmed by new results.[48] As a consequence of Eq. (15), the frequency-dependent optical susceptibility in Eq. (1) takes a simple form. The optical susceptibility of the 2D system with confinement in the y direction changes over into

$$\chi(\omega)=\frac{2}{\varepsilon_0}|\boldsymbol{\mu}|^2L_x\sum_N\left|\int_{-\infty}^{+\infty}dY\,\Phi_N(Y)\right|^2\times\sum_{\hat{\alpha}}\frac{|C^N_{\hat{\alpha}}(0)|^2}{E_g^{\text{2D}}+\varepsilon_N+\varepsilon^N_{\hat{\alpha}}-\hbar(\omega+i\Gamma)} . \tag{16}$$

In the limit of vanishing confinement the well-known 2D optical susceptibility with Coulomb enhancement[24] results. Expression (16) indicates a remarkable spectral redistribution due to the wire confinement. Instead of a one exciton series, as in the 2D case, we expect different absorption edges related to different stages of the center-of-mass motion in the y direction. At each of these edges, exciton series appear. They are themselves modified by the wire confinement. The oscillator strengths of the excitons $\sim|C^N_{\hat{\alpha}}(0)|^2$ in each series are similar to the pure 2D case.

III. EXCITONS IN HARMONIC CONFINEMENT POTENTIALS

For a single quantum wire with complete harmonic confinement in the y direction, i.e., $V_{iy}(y_i)=\frac{1}{2}m_{i\|}\omega_i^2y_i^2$, the transformed confinement potentials defined in Eqs. (9) and (10) are

$$H_{\text{int}}(Y,y)=\mu(\omega_e^2-\omega_h^2)Yy ,$$
$$V_{\text{c.m.}}(Y)=\tfrac{1}{2}M\omega^2_{\text{c.m.}}Y^2,\quad \omega^2_{\text{c.m.}}=\sum_{i=e,h}\frac{m_{i\|}}{M}\omega_i^2 ,$$
$$B^2=\frac{\hbar}{M\omega_{\text{c.m.}}} , \tag{17}$$
$$V_{\text{rel}}(y)=\tfrac{1}{2}\mu\omega^2_{\text{rel}}y^2,\quad \omega^2_{\text{rel}}=\sum_{i=e,h}\frac{\mu}{m_{i\|}}\omega_i^2 ,$$
$$b^2=\frac{\hbar}{\mu\omega_{\text{rel}}} ,$$

where the characteristic wire width $B(b)$ and oscillator frequencies $\omega_{\text{c.m.}}(\omega_{\text{rel}})$ for the center-of-mass (relative) motion is introduced. The Schrödinger equation (12) for the center-of-mass motion of the electron-hole pair perpendicular to the wire can be exactly solved. One has

$$\varepsilon_N=\hbar\omega_{\text{c.m.}}(N+\tfrac{1}{2})\quad(N=0,1,2,\ldots,)$$
$$\Phi_N(Y)=\left[\frac{1}{2^NN!\sqrt{\pi}B}\right]^{1/2}e^{-Y^2/2B^2}H_N\left[\frac{y}{B}\right] . \tag{18}$$

Here $H_N(Y/B)$ denotes the Hermitian polynomial of Nth order. The modification of the oscillator strength of excitonic transitions in Eq. (16) for each stage N of the center-of-mass motion is now simply given by

$$\left|\int_{-\infty}^{+\infty}dY\,\Phi_N(Y)\right|^2=\begin{cases}2\sqrt{\pi}B\left[\dfrac{N}{\frac{N}{2}}\right]\dfrac{1}{2^N} & \text{if } N \text{ even}\\ 0 & \text{if } N \text{ odd} .\end{cases} \tag{19}$$

Accepting the approximations done here, only excitonic transitions with even oscillator quantum numbers of the center-of-mass motion $N=0,2,4,\ldots,$ appear in the optical spectra. The optical selection rule discriminates antisymmetric wave functions $\Phi_N(Y)$. Such even-order quasi-1D exciton transitions seem to be observed in polarization-dependent photoluminescence and photoluminescence excitation spectroscopies[6] for s-polarization, i.e., the electric-field vector of the exciting and detected light is perpendicular to the plane of incidence and parallel to the wires.

Another problem with the oscillator strengths in Eq.

(19) concerns the transition to the exact 2D exciton case, i.e., the vanishing wire confinement. The total strength of all center-of-mass transitions in expression (16) diverges. To avoid this complication, one has to consider that the extent of the xy plane in the y direction is limited by the characteristic length L_y. Approaching the quantum-well case, i.e., $B \to \infty$ (but $B \ll L_y$), the Y integral in Eq. (19) has to be restricted to the interval $-L_y/2 < y < L_y/2$.

By means of the wave functions in Eq. (18) the matrix elements $W_{NN'}(y)$ of the coupling term defined in Eq. (14) can be analytically calculated. One has

$$W_{NN'}(y) = \mu(\omega_e^2 - \omega_h^2)By \times [\sqrt{N/2}\delta_{N',N-1} + \sqrt{N'/2}\delta_{N,N'-1}] . \quad (20)$$

The diagonal elements $W_{NN}(y)$ under consideration vanish and, therefore, do not influence the internal electron-hole pair motion as indicated by Eq. (15). However, in general, the off-diagonal elements in Eq. (20) are also negligible. Even for characteristic extents of the wells of nearly $Y \approx B$ it holds that $|\omega_e - \omega_h| \ll 4E_B/\hbar$ with the binding energy E_B of the corresponding 3D exciton.

Despite this simplification, the equation (15) of internal motion cannot be more analytically solved. In the explicit calculation we do this numerically. Nevertheless, important insight into the structure of the solutions follows expanding the true eigenfunctions $C^N_{\hat{\alpha}}(\mathbf{r})$ in terms of the eigenfunctions of the angular-momentum operator $C^N_{\hat{\alpha}}(\mathbf{r}) = \sum_m f^m_{\hat{\alpha}}(r) 1/\sqrt{2\pi} e^{im\varphi} (m = 0, \pm 1, \pm 2, \ldots,)$. The index N can be omitted and Eq. (15) transforms into a system of radial differential equations

$$\sum_{m'} \left\{ \left[-\frac{\hbar^2}{2\mu} \left(\frac{\partial^2}{\partial r^2} + \frac{1}{r}\frac{\partial}{\partial r} - \frac{m^2}{r^2} \right) - \frac{e^2}{4\pi\varepsilon_0 \varepsilon r} - \varepsilon_{\hat{\alpha}} \right] \delta_{mm'} + \tfrac{1}{2}\mu\omega_{\mathrm{rel}}^2 r^2 \tfrac{1}{4} [2\delta_{m'm} - \delta_{m'm+2} - \delta_{m'm-2}] \right\} f^m_{\hat{\alpha}}(r) = 0 . \quad (21)$$

When the QW confinement effects are smaller than the excitonic effects, more strictly for $(a_B/b)^4 \ll 1$ (a_B is the Bohr radius of the 3D exciton), the confinement potential $\sim r^2$ can be neglected and Eq. (21) changes over into the strict 2D exciton problem[24] for the relative motion. In typical experiments the relation $a_B < b$ is nearly fulfilled. Moreover, the problem of Eq. (21) contains only bound states. Therefore we classify the problem of internal motion by the quantum numbers $\hat{\alpha} = nm$ [$n = 1,2,3, \ldots,$ and $m = 0, \pm 1, \ldots, \pm(n-1) = s, p_\pm, d_\pm, f_\pm, \ldots,$] of the 2D exciton although m is not a good quantum number in the presence of the confinement potential. The index $\pm$ denotes the y parity described by $\cos(m\phi)$ or $\sin(m\phi)$ in the angular-dependent part of the wave functions. This works especially well for the $1s$ ground state. The higher-lying states are, in general, formed by linear combinations of angular-momentum states shifted by multiples of two.

The resulting wave functions $C_{\hat{\alpha}}(\mathbf{r})$ are plotted in Fig. 2 versus the xy plane of an area of $100a_B \times 100a_B$ for four different wire confinements $b = \infty$, $3a_B$, $1.5a_B$, and a_B. In this figure, only the first four quasi-1D excitons $1s$, $2s$, $3s$, and $3d$ appearing in the optical spectra are shown. As can be seen from Eq. (21) the oscillator strengths of the p-, f-, etc., type excitons remain exactly zero since no coupling to the s-type excitons may occur. The same holds for the sine-type d-, g-, etc., type excitons. This property is a result of the symmetry of the wire potential and remains true also for the realistic potentials shown in Fig. 1. Figure 2 shows that the effect of the wire confinement depends remarkably on the extent and the symmetry of the original 2D exciton wave function for $b = \infty$. The increasing confinement down to wire widths of the order of the bulk exciton radius, more strictly $b = a_B$, practically does not influence the $1s$ wave function. The binding of the electron-hole pair in the $1s$ exciton state is rather stable. Even for $b = a_B$ the binding energy is by a factor of 2 larger than the confinement energy $\hbar\omega_{\mathrm{rel}}$. The $2s$ exciton is also rather stable [Fig. 2(b)]. Nevertheless, its radial symmetry is destroyed. Its wave function is compressed in the confinement y direction, whereas its distribution in x direction is broadened along the wire. The maximum after the node splits into two peaks indicating the intermixing with nominal $3d$ states of the 2D exciton. All these effects are more pronounced in the case of the $3s$ exciton [Fig. 2(c)]. A new quality is reached in the case of the quasi-1D exciton with the quantum numbers $3d$ in the exact 2D case ($b = \infty$). Figure 2(d) indicates the intermixing with s excitons and excitons with the quantum number $m = 2$. The most interesting fact is the central peak at $r = 0$ that rises with increasing confinement. It indicates the finite oscillator strength of this exciton induced by the wire confinement.

The confinement effects described for the wave functions can also be discussed for the binding energies and the oscillator strengths of the quasi-1D excitons. They are plotted in Figs. 3 and 4 versus the characteristic length b of the wire confinement potential for the relative motion. In the case of the nominal $1s$ excitons neither the binding energy nor the oscillator strength are essentially influenced by the wire confinement, at least in the interval $a_B \leq b < \infty$. They keep their 2D values, $4E_B$ and $16/a_B^2$. As in the case of the wave functions the influence of confinement is much stronger for the other excitons. The Coulomb degeneracy is lifted, as explicitly shown for $3s$ and $3d$ in Fig. 3. The peak positions of these excitons are displaced to higher energies. For a certain confinement, i.e., b, these peak positions are already above the continuum edge of the 2D problem indicating that the binding energies of these excitons are smaller than the wire confinement energy $\hbar\omega_{\mathrm{rel}}$. A very interesting behavior is found for the oscillator strength, more strictly for $|C^N_{\hat{\alpha}}(0)|^2$. In the case of $2s$ its value decreases somewhat with rising a_B/b indicating a loss of strength to the formerly forbidden excitons. The oscillator strengths of the nominal $3s$ and $3d$ show a remarkable in-

crease. The $3d$ exciton, that is forbidden in the exact 2D case, even becomes a larger strength than the $2s$ one. In the limit $b \to \infty$, linear combinations of the $3s$ and $3d$ cosine-type wave functions remain which coefficients are given by first-order degenerate perturbation theory. However, in Figs. 2(c) and 2(d) in the case $b = \infty$ the pure $3d$ and $3s$ excitons are shown, in agreement with the usual consideration.

IV. OPTICAL SPECTRA

A. Harmonic confinement and line shape

The imaginary part of the optical susceptibility $\chi(\omega)$ is calculated by means of expression (16). For this purpose, the center-of-mass equation (12) and Eq. (15) for the internal motion are solved numerically. We choose an energy region near and somewhat above the lowest heavy-hole electron transition of the underlying quantum-well structure. The spectrum resulting within the harmonic confinement model and complete e-h symmetry is plotted in Fig. 5 for different wire confinements $\hbar\omega_{\text{c.m.}} = 0$, 0.5, 1, 1.5, and $2E_B$. The values for the internal motion are $b = \infty$, 2, 1.41, 1.15, and $1a_B$. These energies and lengths have to be compared with the binding energy $E_{\text{exc}} = 4E_B = 20$ meV and Bohr radius $a_{\text{exc}} = a_B/2 = 57$ Å of the underlying 2D exciton if one applies $\varepsilon = 12.9$ for GaAs.[31]

The stronger influence of the wire confinement on the center-of-mass motion is clearly seen in the spectra of Fig. 5. The single $1s$ 2D exciton peak at zero center-of-mass momentum decays very rapidly into different nearly

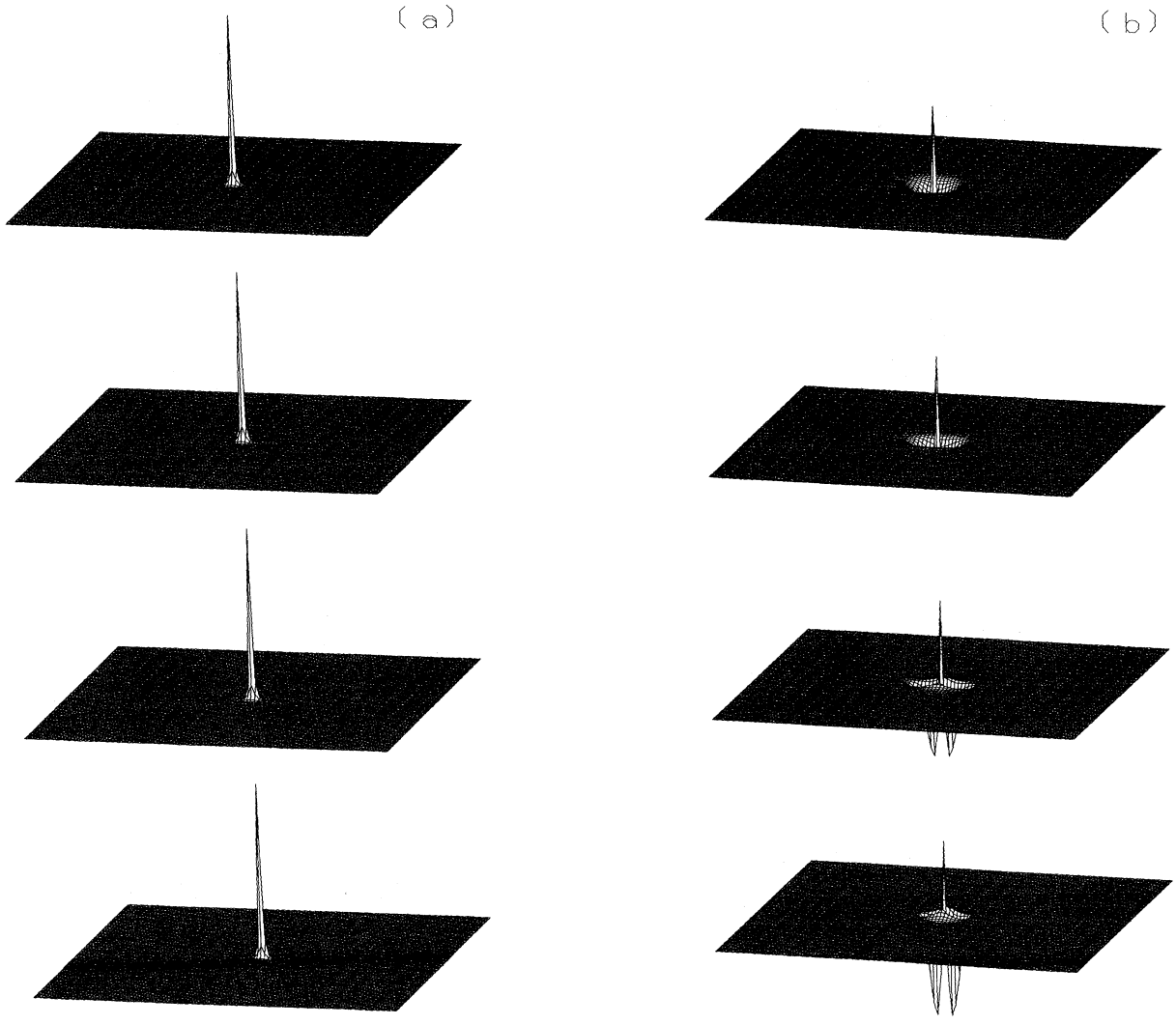

FIG. 2. Wave functions of the internal motion of 2D excitons in an additional harmonic confinement potential representing the quantum wire. (a) $1s$, (b) $2s$, (c) $3d$, and (d) $3s$ where the notation of the 2D excitons is kept. The harmonic confinement is described by the characteristic lengths $b = \infty$, 3, 1.5, and $1a_B$.

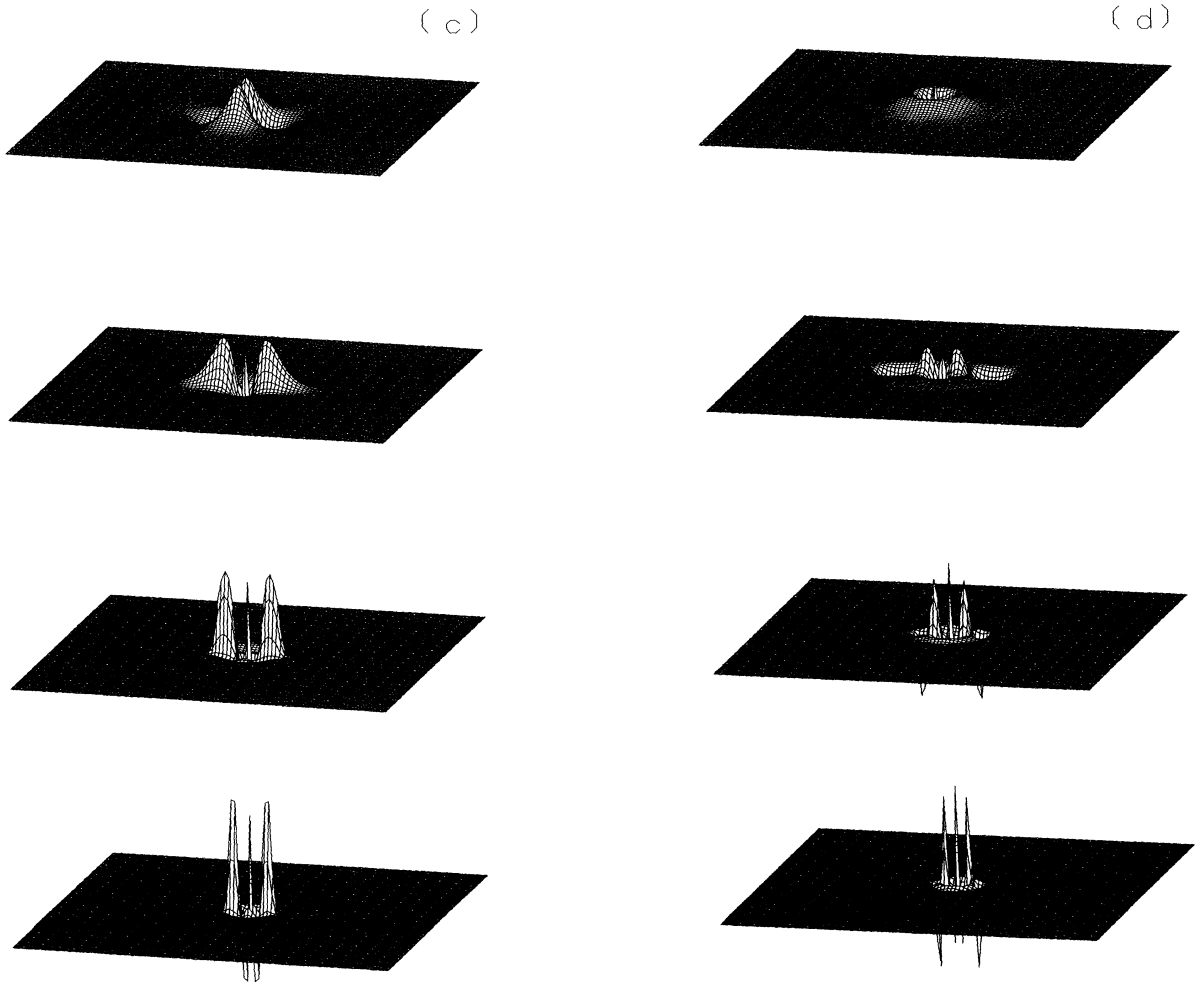

FIG. 2. (*Continued*).

equidistant 1*s* exciton peaks with quantum numbers $n=0,2,4,\ldots$. Their energetic distance is $\hbar\omega_{\text{c.m.}}$. With increasing confinement, the first main peak is blueshifted to higher energies by the zero-point energy $\frac{1}{2}\hbar\omega_{\text{c.m.}}$. When $\hbar\omega_{\text{c.m.}}$ exceeds lifetime broadening, single exciton lines appear, even eventually above the 2D continuum edge E_g^{2D} (the energy zero point in Fig. 5) if $\hbar\omega_{\text{c.m.}}(N+\frac{1}{2})>4E_B$. Their oscillator strengths are distributed according to expression (19).

The fine structure of the exciton lines is governed by

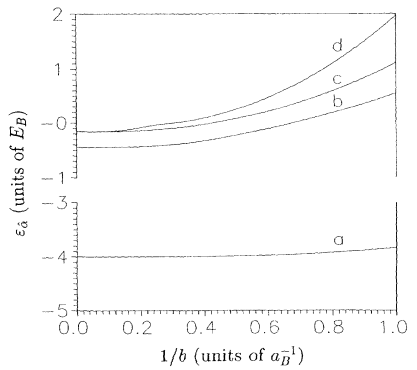

FIG. 3. Energies of quasi-1D excitons vs wire confinement without the effect of the center-of-mass quantization. The zero indicates the position of the 2D energy gap. (a) 1*s*, (b) 2*s*, (c) 3*d*, and (d) 3*s*.

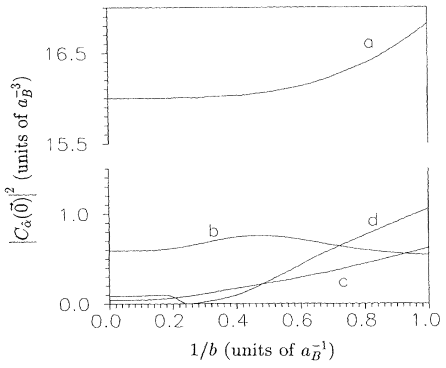

FIG. 4. Oscillator strengths of quasi-1D excitons vs wire confinement. The quantization stage of the center-of-mass motion is fixed. (a) 1*s*, (b) 2*s*, (c) 3*d*, and (d) 3*s*.

the ratio of the effective wire width b with respect to the internal motion and the Bohr radius a_B. For $b \gg a_B$, no fine structure occurs. In the region $b \geq a_B$ the Coulomb degeneracy is lifted as shown in Fig. 3. The split exciton lines belonging to the main nominal $1s$ peak with a quantum number N appear at energies shifted nearly by $E_{\text{exc}}=4E_B$. Therefore, in general, they apparently follow main peaks with a different quantum number N. In the case $b \leq a_B$, a reverse tendency can be observed. The motions of electron and hole are nearly independent and govern the shape of the spectra. The Coulomb potential couples such electron and hole states and, hence, again produce a fine structure in the optical spectra.

B. Wire fabrication and potential shape

We apply the realistic potentials shown in Figs. 1 and 6. We take into account that the sample consists of an

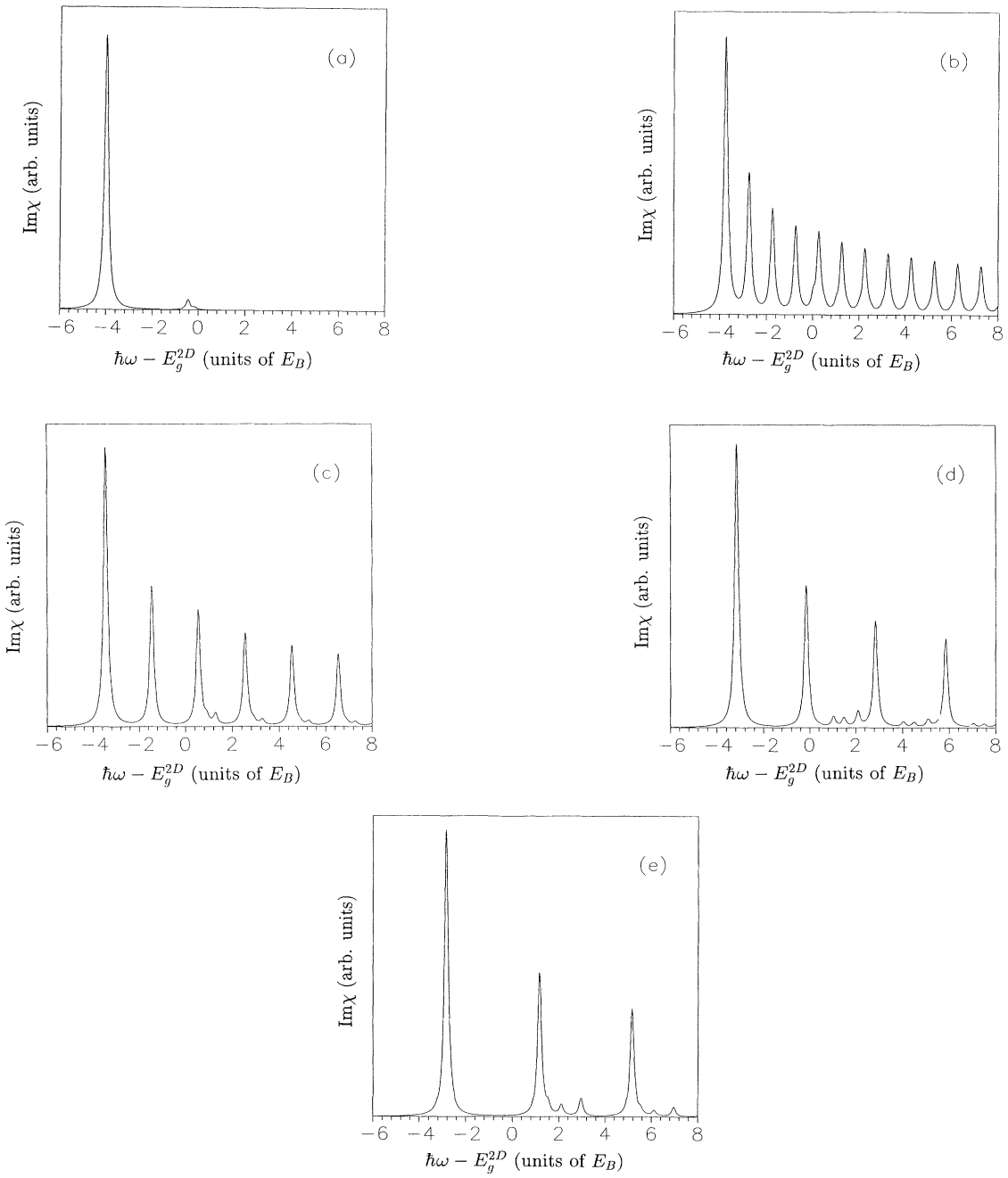

FIG. 5. Imaginary part of the optical susceptibility for a single quantum wire and harmonic confinement. The inverse lifetime of the excitons is fixed at $\Gamma=0.1E_B$. $\hbar\omega_{\text{c.m.}}=0$ (a), 0.5 (b), 1 (c), 1.5 (d), and $2E_B$ (e).

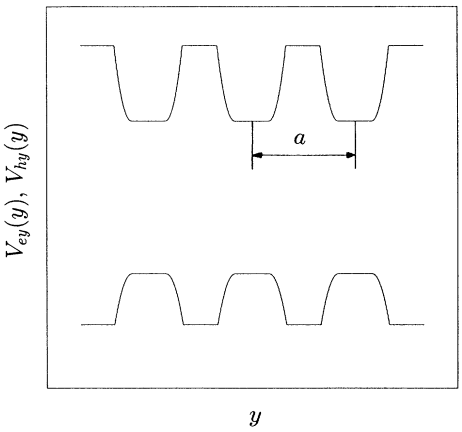

FIG. 6. The continuation of the electron and hole confinement potentials for a periodic array of wires in the distance a along the y direction.

array of QW's in a distance a. However, the overlap of wave functions localized in wells at different positions are neglected. Nevertheless, the parameter a is used to discuss the shape of the single electron and hole potentials shown in Fig. 1. Thereby we try to model the situation of a QW array fabricated by means of the laser-induced interdiffusion of cations in GaAs well layers and $Al_xGa_{1-x}As$ barrier layers.[8]

In this way we find depths of the electron and hole confinement potentials in y direction that are characterized by band discontinuities $\Delta E_c(x_W)$ and $\Delta E_v(x_W)$. The composition $x_W(0<x_W<x)$ is that of the $Al_{x_W}Ga_{1-x_W}As$ in the wire barriers in the y direction formed by interdiffusion. We assume $\Delta E_c(x)=0.6\Delta E_g(x)$ and $\Delta E_v(x)=0.4\Delta E_g(x)$ (Ref. 49) with $\Delta E_g(x)=1.155x+0.37x^2$ (Ref. 50) as the difference in the band gaps between GaAs and $Al_xGa_{1-x}As$ in the $x<0.4$ region and for low temperature.

In the experiment of Brunner *et al.*[8] a GaAs well layer of 30-Å thickness is interdiffused with 200-Å-thick $Al_xGa_{1-x}As$ barriers ($x=0.35$). Therefore a maximum Al content of the wire barriers of $x_W=0.25$ is expected for complete local interdiffusion. In practice, the interdiffusion is not complete and, moreover, spatially not homogeneous. Hence, the average values of x_W in the barriers are always smaller than 0.25, i.e., $\Delta E_c<187$ meV and $\Delta E_v<125$ meV. From the appearance of quantization structures in the photoluminescence spectra[8] (cf. inset in Fig. 7 of Ref. 8) maximum barriers of about 35 meV follow indicating a maximum Al content in the wire barriers of $x_W\approx 0.05$ on the average.

The width of the interdiffusion profile in the y direction along the laser scan line, i.e., nearly the width of the QW barrier, is about 100 nm.[8] Together with the band discontinuities it determines the slope of the potential wells for electrons and holes. Assuming equal total width and equal width l of the well bottom one has $\omega_e^2/\omega_h^2=\Delta E_c m_{h\parallel}/\Delta E_v m_{e\parallel}$, i.e., $\omega_e=3.29\omega_h$. The total wire width is then $[2\Delta E_c/(m_{e\parallel}\omega_e^2)]^{1/2}$. $\hbar\omega_{\text{c.m.}}$ follows from the energetic distances of the main peaks in the luminescence spectra.[8] One has $\omega_e=2.22\omega_{\text{c.m.}}$, $\omega_h=0.675\omega_{\text{c.m.}}$ and $\omega_{\text{rel}}=2.10\omega_{\text{c.m.}}$. Consequently, three parameters $\omega_{\text{c.m.}}$, l, and x_W appear in the explicit calculations. $\omega_{\text{c.m.}}$ is taken from the experiment, l is really a fit parameter, and x_W is only implicitly taken into account to restrict the number of quantized levels in the center-of-mass as well as internal motion by fixing ΔE_c and ΔE_v.

The picture of the wire potentials realized by laser-induced cation interdiffusion and described above remains valid as long as the double diffusion length of about 180 nm is smaller than the wire distance. Otherwise, the bottom width l is zero or even formally negative. The latter case $l<0$ means that pure GaAs is not more present in the wire region. Rather, $Al_xGa_{1-x}As$ with an Al content $x<x_W$ appears. We describe this fact by an increase of the 2D energy gap E_g^{2D} by $\Delta E_g(x)$ and a corresponding decrease of the well depths ΔE_c and ΔE_v.

C. Comparison with luminescence spectra

The imaginary part of the optical susceptibility (16) calculated by means of realistic wire potentials as described in Sec. IV B is plotted in Fig. 7. The finite depth of the wells and the occupation dependence of the luminescence are simulated restricting the number of involved levels of center-of-mass and internal motion by 40 meV. In such a way the theoretical curves can be compared with experimental luminescence spectra.[8]

In this figure the pure 2D case comes out in the limit $l=\infty$. In the considered energy region only the strong luminescence via the $1s$ excitons of the first heavy-hole valence subband to conduction subband is seen. In the theoretical spectrum the very small $2s$ exciton luminescence is additionally seen. With decreasing well width l the internal motion of the $1s$ exciton remains hardly influenced by the wire quantization. Particularly, replicas ($N=2,4,\ldots,$) of the main peak ($N=0$) appear due to the center-of-mass quantization. Their oscillator strengths decrease with rising N. They are $1,\frac{1}{2},\frac{3}{8},\frac{5}{16},\ldots$, for $N=0,2,4,6,\ldots$, at least in the complete harmonic limit. For $l=0$ the situation changes drastically. A blueshift of the two-particle ground state becomes visible and the fine structure of each peak with different N caused by the internal motion appears. The detailed interpretation of the resulting spectrum is complicated because peaks related to the lifted Coulomb degeneracy in the internal exciton motion and belonging to a particular stage N of the center-of-mass motion occur at positions shifted by about E_{exc} to higher energies. In this way, for typical quantization energies of the center-of-mass motion smaller than the 2D exciton binding energy, they are observed between peaks with quantum numbers N' and $N'-2$ different from N. The case of nominal negative l is characterized by a remarkable blueshift of the spectrum. In the explicit calculation, we describe this fact by an enlarged 2D band gap E_g^{2D}.

Our series of theoretical spectra is in qualitative agreement with the measurements of Brunner *et al.*[8] This

holds, in principle, with respect to the position and the number of peaks. Because of our rigorous 2D approximation accompanied by a restriction of the particle motions in the xy plane, the excitonic effects in the underlying quantum-well structure are somewhat overestimated. This defect may be partially lifted by shifting the $1s$ exciton luminescence peak for $l=\infty$ into the experimental position at nearly $\hbar\omega=1.69$ eV. Another discrepancy between theory and experiment concerns the variety of peaks for smaller distances $a=200$ and 150 nm of the wires and, therefore, rather narrow wires. In the measured luminescence spectra more peaks can be observed and, respectively, the first peaks are split. We believe that the absence of the split peaks in the theoretical curves can be traced back to the neglect of overlap effects. More strictly speaking, besides the direct excitons with electrons and holes in the same wire, spatially indirect excitons[51] belonging to excitons with electron

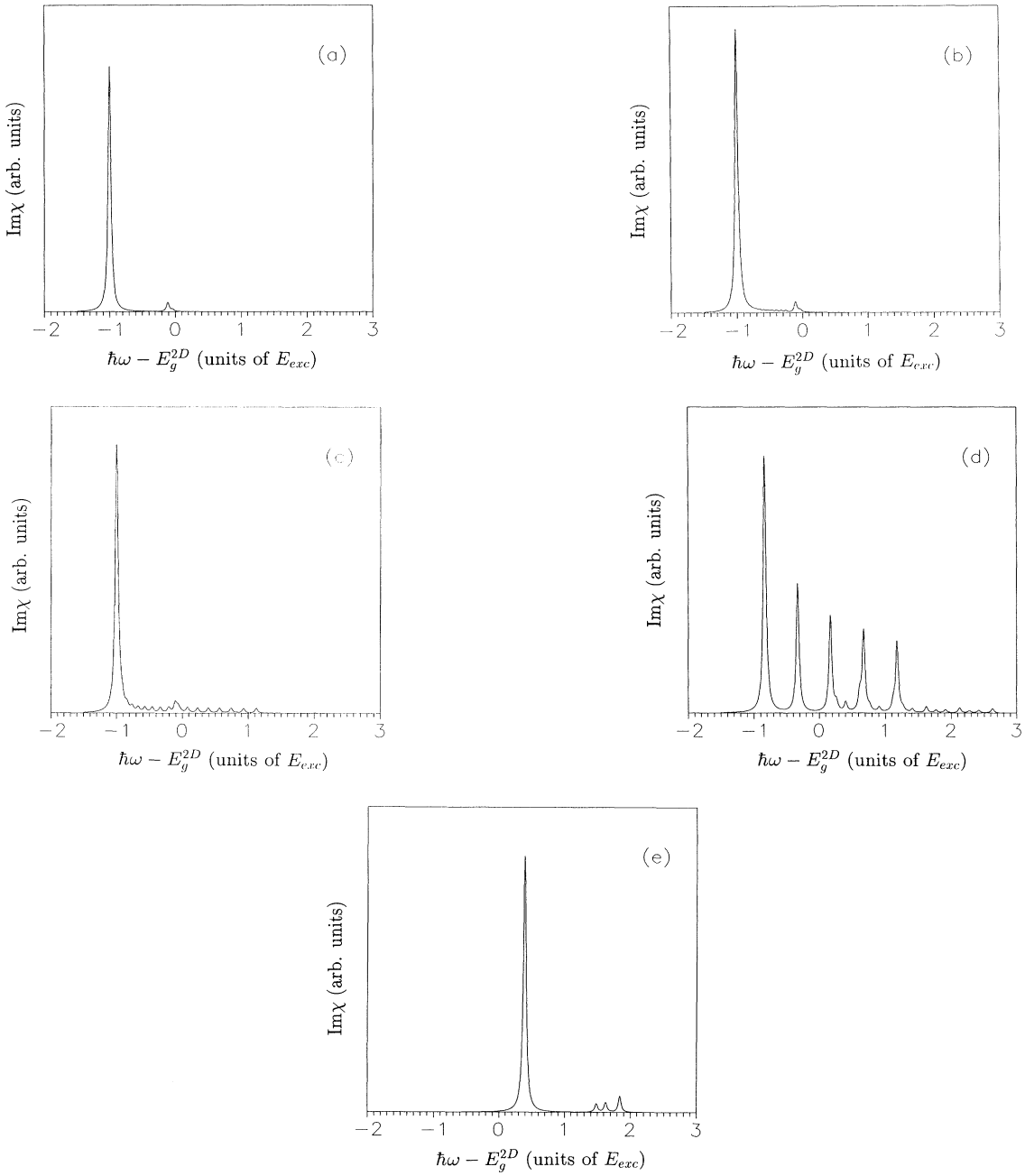

FIG. 7. Theoretical photoluminescence spectra calculated for an array of quantum wires with different confinement potentials as indicated by different bottom widths $l=\infty$ (a), 20 (b), 10 (c), 0 (d), and $-2.5a_B$ (e). The exciton lifetime is fixed as in Fig. 5.

and hole in neighbored wires appear in the luminescence. Other possibilities of explanation concern a more complicated shape of the particle confinement potentials over the wire array as a consequence of the diffusion processes. There can be additional wells within the nominal barrier regions between two wires or fluctuations in wire shapes themselves. The latter reason seems to be more relevant. Scanning the photoluminescence probe across the wire structures of narrow period $a \leq 200$ nm samples reveal some inhomogeneities.

A striking difference between experiment and theory concerns the linewidths. The luminescence lines are much broader than the assumed lifetime broadening of $\Gamma = 0.025 E_{\text{exc}}$, especially for larger wire distances a and, hence, wire widths. Two important effects are not included in the theory with constant small Γ. (i) In the experiment, one finds a variation from $\Gamma \approx 4$ meV for the 2D excitons to $\Gamma \approx 1$ meV for the quasi-1D exciton in the case of $a = 200$ nm. (ii) The experimental lines seems to be inhomogeneously broadened by fluctuations in the wire shapes.

V. SUMMARY

In conclusion, we have demonstrated the transition from the complete 2D exciton in an extremely narrow quantum well to a quasi-1D exciton in well-separated quantum wires prepared on the base of a narrow quantum well. The transition is characterized by the interplay of the center-of-mass motion of the electron-hole pair, its internal motion associated with exciton binding, and the confinement of electron and hole due to the wire potentials.

In the case of harmonic wire confinement with a characteristic length b of the displacement of the corresponding oscillator, the strengths of the different effects can be discussed comparing b with the Bohr radius a_B. (i) For $b \gg a_B$, the 2D exciton peak splits due to the quantization of the center-of-mass motion. The oscillator strength is distributed over the different peaks belonging to symmetric wave functions and a blueshift appears. The relative motion of electron and hole remains 2D-like. (ii) In the region $b \geq a_B$, the Coulomb degeneracy in the relative exciton motion is lifted. Nominal 2D excitons with angular-momentum quantum number $m = 0, 2, 4, \ldots$, couple and the peaks exhibit a fine structure. (iii) When wire confinement effects overcome excitonic effects, i.e., $b \leq a_B$, the motions of electron and hole are nearly independent and govern the line shape. The Coulomb potential couples such electron and hole states and produces a fine structure in the optical spectra.

Our results are applied to explain recent photoluminescence spectra of wire systems with varying wire widths and wire distances. The development of photoluminescence near the lowest heavy-hole conduction-band transition from wire arrays produced by laser-induced cation interdiffusion with the array parameters is interpreted in terms of the interplay of excitonic effects and wire confinement. The spectrum for near wires, especially its strong blueshift, can only be explained assuming a shift of the 2D gap to higher energies and, therefore, already a $Ga_xAl_{1-x}As$ with a very small Al content in the wire regions.

ACKNOWLEDGMENTS

We would like to thank G. Abstreiter, K. Brunner, D. Heitmann, H. Lage, and R. Zimmermann for helpful discussions.

[1] Y. Hirayama, S. Tarucha, Y. Suziki, and H. Okamoto, Phys. Rev. B **37**, 2774 (1988).
[2] D. Gershoni, H. Temkin, G. J. Dolan, J. Dunsmuir, S. N. G. Chu, and M. B. Panish, Appl. Phys. Lett. **53**, 995 (1988).
[3] M. Tsuchiya, J. M. Gaines, R. H. Yan, R. J. Simes, P. O. Holtz, L. A. Coldren, and P. M. Petroff, Phys. Rev. Lett. **62**, 466 (1989).
[4] M. Kohl, D. Heitmann, P. Grambow, and K. Ploog, Phys. Rev. Lett. **63**, 2124 (1989).
[5] M. Tanaka, J. Motohisa, and H. Sakaki, Surf. Sci. **228**, 408 (1990).
[6] H. Lage, D. Heitmann, R. Cingolani, P. Grambow, and K. Ploog, Phys. Rev. B **44**, 6550 (1991).
[7] R. Cingolani, H. Lage, L. Tapfer, H. Kalt, D. Heitmann, and K. Ploog, Phys. Rev. Lett. **67**, 891 (1991).
[8] K. Brunner, G. Abstreiter, M. Walter, G. Böhm, and G. Tränkle, Surf. Sci. **267**, 218 (1992).
[9] M. Kohl, D. Heitmann, W. W. Rühle, P. Grambow, and K. Ploog, Phys. Rev. B **41**, 12 388 (1990).
[10] K. Kash, J. Lumin. **46**, 69 (1990).
[11] J. A. Brum and G. Bastard, Superlatt. Microstruct. **4**, 623 (1988).
[12] D. S. Citrin and Y. C. Chang, Phys. Rev. B **40**, 5507 (1989); J. Appl. Phys. **68**, 161 (1990).
[13] P. C. Sercel and K. J. Vahala, Phys. Rev. B **42**, 3690 (1990).
[14] G. A. Baraff and D. Gershoni, Phys. Rev. B **43**, 4011 (1991).
[15] Y. Arakawa, T. Yamauchi, and J. N. Schulman, Phys. Rev. B **43**, 4732 (1991).
[16] M. Asada, Y. Miyamoto, and S. Suematsu, Jpn. J. Appl. Phys. **24**, L95 (1985).
[17] J. W. Brown and H. N. Spector, Phys. Rev. B **35**, 3009 (1987).
[18] D. A. B. Miller, D. S. Chemla, and S. Schmitt-Rink, Appl. Phys. Lett. **52**, 2154 (1988).
[19] J. Lee and M. O. Vassell, Phys. Rev. B **42**, 5274 (1990).
[20] P. C. Sercel and K. J. Vahala, Phys. Rev. B **44**, 5681 (1991).
[21] U. Bockelmann and G. Bastard, Europhys. Lett. **15**, 215 (1991); U. Bockelmann (unpublished).
[22] D. S. Citrin and Y.-C. Chang (unpublished).
[23] R. J. Elliott, Phys. Rev. **108**, 1384 (1957).
[24] M. Shinada and S. Sugano, J. Phys. Soc. Jpn. **21**, 1936 (1966).
[25] T. Kodama and Y. Osaka, Jpn. J. Appl. Phys. **25**, 1875 (1986).
[26] L. Banyai, I. Galbraith, C. Ell, and H. Haug, Phys. Rev. B **36**, 6099 (1987).
[27] J. W. Brown and H. N. Spector, Phys. Rev. B **35**, 3009 (1987).
[28] M. H. Degani and O. Hipolito, Phys. Rev. B **35**, 9345 (1987).
[29] A. D'Andrea and R. Del Sole, Solid State Commun. **74**, 1121 (1990).
[30] T. Ogawa and T. Takagahara, Phys. Rev. B **43**, 14 325 (1991); **44**, 8138 (1991).
[31] R. Zimmermann, *Many-Particle Theory of Highly Excited*

Semiconductors (Teubner-Verlag, Leipzig, 1987).

[32]The separation of the luminescence intensity $I(\omega)$ [Eq. (2)] into the Bose function and the susceptibility is only exact within a two-band model. Nevertheless, we approximately apply this decoupling assuming a near independence of the subband transitions in the wire system under consideration.

[33]H. Haug and S. W. Koch, *Quantum Theory of the Optical and Electronic Properties of Semiconductors* (World Scientific, Singapore, 1990).

[34]L. Wendler, F. Bechstedt, and M. Fiedler, Phys. Status Solidi B **159**, 143 (1990); Superlatt. Microstruct. **10**, 183 (1991).

[35]H.-R. Trebin, U. Rössler, and R. Ranvaud, Phys. Rev. B **20**, 686 (1979).

[36]C. Trallero-Giner, T. Ruf, and M. Cardona, Phys. Rev. B **41**, 3028 (1990).

[37]M. Altarell, in *Heterojunctions and Semiconductor Superlattices,* edited by G. Allan, G. Bastard, N. Boccara, M. Lannoo, and M. Voos (Springer-Verlag, Berlin, 1986).

[38]G. Harbeke, O. Madelung, and V. Rössler, in *Physics of Group IV Elements and III-V Compounds,* edited by O. Madelung, M. Schulz, and H. Weiss, Landolt-Börnstein New Series, Group III, Vol. 17, Pt. A (Springer-Verlag, Berlin, 1982).

[39]R. Loudon, Am. J. Phys. **27**, 649 (1959).

[40]R. J. Elliott and R. Loudon, J. Phys. Chem. Solids **8**, 382 (1959); **15**, 196 (1960).

[41]G. Y. Hu and R. F. O'Connel, Phys. Rev. B **36**, 5798 (1987).

[42]T. Demel, D. Heitmann, P. Grambow, and K. Ploog, Phys. Rev. B **38**, 12 732 (1988).

[43]Q. Li and S. Das Sarma, Phys. Rev. B **40**, 5860 (1989).

[44]J. K. Jain and S. Das Sarma, Phys. Rev. B **36**, 5949 (1987).

[45]G. Y. Hu and R. F. O'Connel, Phys. Rev. B **42**, 1290 (1990).

[46]S. Glutsch, F. Bechstedt, and R. Zimmermann, in *Proceedings of the International Meeting on Optics of Excitons in Confined Systems, Giardini Naxos 1991,* edited by A. D'Andrea, R. Del Sole, R. Girlanda, and A. Quattropani (The Institute of Physics, Bristol, 1992), p. 293; Phys. Status Solidi B **172**, 357 (1992).

[47]V. Hanonen, in (Ref. 46), p. 313.

[48]S. Glutsch and F. Bechstedt, Phys. Rev. B (to be published).

[49]R. C. Miller, A. C. Gossard, D. A. Kleinman, and O. Munteanu, Phys. Rev. B **29**, 3740 (1984); R. C. Miller, D. A. Kleinman, and A. C. Gossard, *ibid.* **29**, 7085 (1984).

[50]S. Adachi, J. Appl. Phys. **58**, R1 (1985).

[51]F. Hirler, R. Küchler, R. Strenz, G. Abstreiter, G. Böhm, J. Smoliner, G. Tränkle, and G. Weimann, Surf. Sci. **263**, 536 (1992).